Thermal Conductivity of Rubber Compounds Versus the State of Cure

Zied Cheheb, Pierre Mousseau, Alain Sarda, Rémi Deterre*

The thermal conductivity of a rubber compound is studied as a function of its state of curing. The device is presented and the calculations in order to obtain samples with controlled and homogeneous vulcanization rates are performed. The hot disk technique is used to measure the thermal conductivity of the rubber. This transient, plane-source and non-destructive method allows rapid and accurate measurement of the thermal conductivity based on the measurement of the electrical resistance of a plane sensor placed between two identical samples. The obtained results show that the thermal conductivity may vary significantly as a function of vulcanization rate. The effect of this variation on the prediction of the reaction progress is discussed.

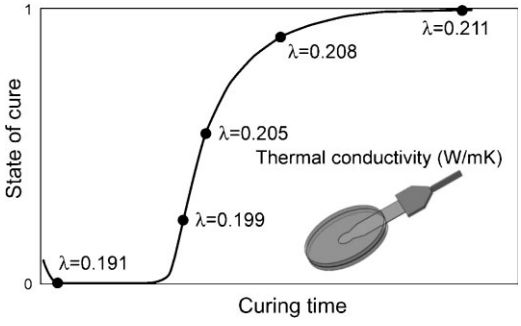

Introduction

The mechanical and structural properties of a molded rubber sample are conditioned by the vulcanization rate achieved at the end of the curing process.[1] Elastomers are mostly composed of polymer molecules compiled on partially entangled chains.[2] A non-vulcanized compound is characterized by a plastic behavior generated by relative sliding between chains occurring during the application of mechanical stress. During vulcanization, a three-dimensional network is formed by links created between macromolecules, thus preventing the chains from sliding and large relative motions. The vulcanization process is at the origin of the elastic behavior of vulcanized rubber parts. The macromolecular network model can explain the elastic behavior of vulcanized rubber and the dependence of the mechanical properties on vulcanization rate.[3]

Z. Cheheb, P. Mousseau, A. Sarda, R. Deterre
LUNAM Université, IUT de Nantes, CNRS, GEPEA, UMR 6144, OPERP ERT1086, 2 avenue du Professeur Jean Rouxel, BP 539, 44475 Carquefou Cedex, France
E-mail: remi.deterre@univ-nantes.fr

The vulcanization rate depends on the thermal history of the rubber compound that arises from the thermal transfers occurring during the molding process.[4] Thermal energy must be provided to the rubber compound in order to reach high vulcanization rates in the material. Heat transfer controls the curing progress by governing chemical reactions through the molded samples. Such dependence is particularly important in the case of thick samples in which the low thermal conductivity of rubber generates important temperature gradients.

The control of the properties of a molded rubber part requires the control of the vulcanization rate distribution. Such control requires the knowledge of the thermal history of the compound through the entire process.[5] Previous work[6] has shown that it is possible to determine the thermal molding parameters in order to obtain a desired vulcanization rate through thick molded rubber parts.

The molding parameter optimization method described previously[6] requires the use of a reliable prediction model for the thermal and kinetic history of the molded compound. The quality prediction depends strongly on the accuracy of the thermophysical parameters, especially the thermal conductivity.[7] For the same polymer sample, the available values for the thermal conductivity show important differences depending on the measurement

DOI: 10.1002/mame.201100127

technique and experimental conditions. Consequently, it is necessary to ensure the quality of measurement of this thermal parameter in order to reach an accurate prediction of the vulcanization rate within the rubber molded parts. In addition, the evolution of the thermal conductivity of a rubber molded part as a function of molding parameters (temperature and pressure) and vulcanization progress must be considered. Several works deal with the temperature,[7–11] pressure,[12–16] and filler[17,18] effect on thermal conductivity evolution of rubber compounds.

To our knowledge, there is no study available dealing with the effect of vulcanization rate on the thermal conductivity of a rubber compound. However, some publications assume that this dependence is weak.[19]

In this work, we detail the theoretical approach and the experimental process used in order to obtain molded rubber samples with controlled and homogeneous vulcanization rates (called iso-α samples). A differential scanning calorimeter (DSC) is used to measure the final state of cure of the molded parts. Then, we describe the thermal conductivity measurement and present the result showing the evolution of the thermal conductivity of the studied compound as a function of the vulcanization rate. The last section is devoted to the study of the effect of the obtained results on the quality of prediction models.

Experimental Section

Molding of Iso-α Samples

The curing state of a rubber part is a direct result of the applied thermal cycle. An optimization method of the curing cycles in order to obtain thick rubber part with a controlled and homogeneous vulcanization rate was presented by El Labban.[6] This method was based on a numerical modeling of the curing process associated to an inverse optimization method. The numerical model was developed on COMSOL Multiphysics software. The aim was to find out an optimal cycle from a desired distribution of the vulcanization rate through the sample thickness. An inverse estimation procedure was used to obtain a typical heating cycle (Figure 1). The thermal cycles corresponding to one desired vulcanization rate were then obtained by changing the coordinates: the time and temperatures of the characteristic points (T_i,t_i) of the typical cycle. Curing cycle parameters allowing the molding of samples with vulcanization rates of 0.25, 0.5, 0.8, and 1, respectively, are presented in Table 1. The obtained samples are called iso-α samples.

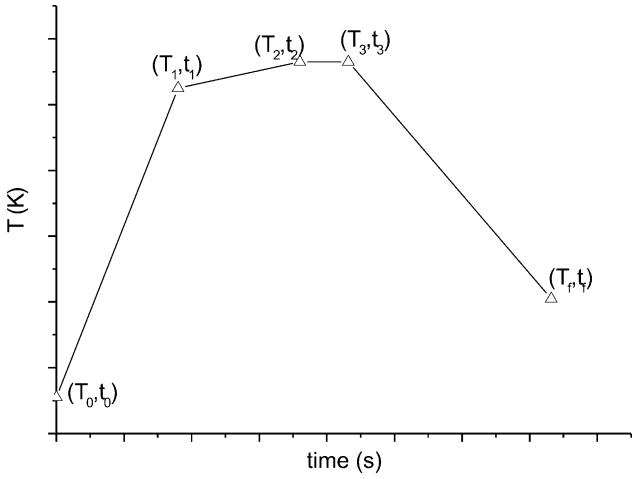

Figure 1. Typical thermal curing cycle of an iso-α sample.

The mold used in order to obtain the iso-α samples is presented in Figure 2. This was a compression mold with a cylindrical part cavity of 100 mm diameter and 5 mm thickness (Figure 3). The thermal regulation of the mold (Figure 2) included a heating and a cooling systems.[20] Heating power was provided by two double spiral electrical resistors [(a) in Figure 2] associated with two electrical power suppliers of 1 200 W. The cooling system was based on two compressed air channels controlled by two solenoids and powered by an air compressor providing a controlled air pressure in the cooling circuit [(b) in Figure 2]. Heating and cooling systems were symmetrical with respect to the median plane of the sample [(c) in Figure 2]. The circuit design was optimized to ensure a uniform heat flux on the surface of the rubber part during molding. The curing system was controlled by two thermal regulators through a graphical computer interface. The lateral surface of the cavity was thermally insulated with composite material (Deltherm) to insure a one directional heat transfer across the sample during curing cycle. The real temperatures of the curing cycles (T_{up} and T_{low}, Figure 2) were measured by two thermocouples located on the upper and the lower sides of the sample. The pressure required for the molding process was provided by a REP V39 rubber injection molding machine. The press plates [(d) in Figure 2d] remained at room temperature throughout the curing cycle.

The curing states for the different molded parts were verified by measuring the residual enthalpy of the samples and by comparing it to the vulcanization enthalpy of a raw sample.[21]

Table 1. Curing cycles calculated for the different vulcanization rates samples.

α_i (target)	T_0 [K]	T_1 [K]	t_1 [s]	T_2 [K]	t_2 [s]	T_3 [K]	t_3 [s]	T_f [K]	t_f [s]
0.25	291	385	1 800	393	3 600	393	4 320	321	7 320
0.5	291	391	2 580	391	4 500	391	5 580	340	7 200
0.8	291	389	1 800	397	3 600	379	4 080	321	7 500
1	291	404	2 580	404	4 500	404	5 580	340	7 200

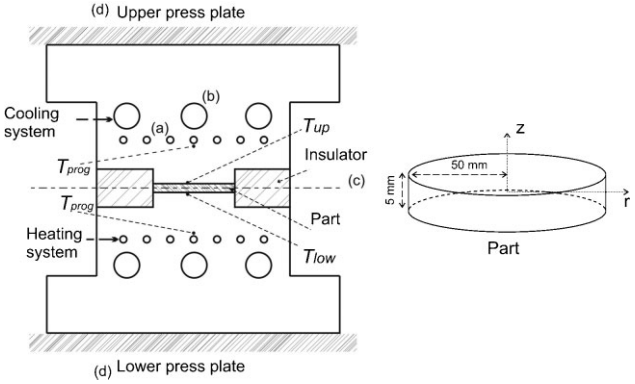

Figure 2. The experimental device used.

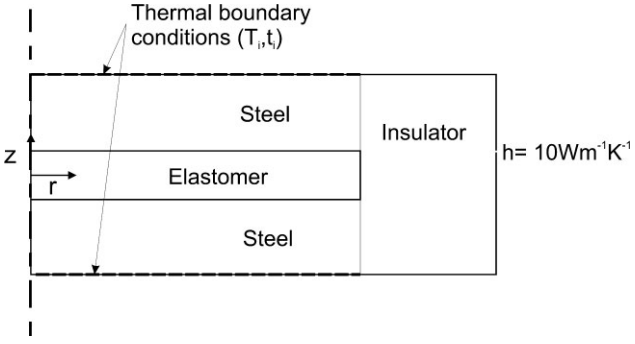

Figure 3. 2D numerical model for cylindrical part curing.

Enthalpies for samples taken from the iso-α molded parts were measured using a DSC Perkin-Elmer 8500. Samples were taken through the thickness of the parts particularly in the middle of the part ($z = 0$, Figure 3) where the state of cure is more homogeneous.

Aluminum crucibles of 50 μL were used, the samples weights were 18.26, 19.26, 16.94, and 31.26 mg for the samples of vulcanization target rates (α_i) of 0, 0.25, 0.5, and 0.8, respectively. The same heating cycle was applied for all DSC measurements: a temperature increase from 40 to 260 °C with a 20 °C · min^{-1} heating rate. Three measurements were performed for each iso-α sample under nitrogen atmosphere with a 20 mL · min^{-1} flow rate.

Thermal Conductivity Measurements

The thermal conductivities of the molded iso-α parts were measured with a TPS 2500 HotDisk AB system based on the transient hot disk technique.

The hot disk measurement is based on a transient plane source technique, developed by Gustafsson et al.,[22–24] allowing a simultaneous measurement of the thermal conductivity and the thermal diffusivity. Since 2008, the hot disk technique has become standard method used for the thermal conductivity measurement of plastic materials.[25] The thermal properties of plastic materials are quite similar to those of the materials used in this work. The measurement technique[26–29] was based on the use of a thin disk sensor composed of a nickel double spiral sealed between two thin insulator Kapton films. The sensor diameter was selected according to the sample dimensions in order to meet the semi-infinite sample assumption required for this technique. A small constant electrical power was applied to the sensor sandwiched between two identical samples (Figure 4). The heating of the sensor due to joule effect causes a symmetrical heating power on both parts of the sample. The temperature increase of the sensor was accurately determined by measuring its electrical resistance [Equation 2],

$$R(t) = R_0\left[1 + \upsilon\Delta\overline{T}(t)\right] \tag{1}$$

where R is the electrical resistance of the sensor, R_0 its resistance at the initial temperature, and υ is the temperature coefficient of the sensor.

The temperature increase of the sensor depends on the heating power and on the thermal properties of the sample that surrounds it.

The applied heat power through the sensor is treated as an internal heat source of strength Q. The heat transfer within the sample is then governed by

$$a\nabla^2 T + \frac{Q}{\rho C} = \frac{\partial T}{\partial t} \tag{2}$$

where a is the thermal diffusivity, ρ the density, and C is the specific heat capacity.

An exact general solution for the heat transfer equation with heat source of strength Q is given by

$$T(r,t) = T_0 + \int_0^t \int_{V'} \frac{Q(\xi,t)}{\rho C} \frac{1}{[4\pi a(t-t')]^{3/2}} \exp\left(-\frac{(r-\xi)^2}{4a(t-t')}\right) \mathrm{d}^3\xi\,\mathrm{d}t' \tag{3}$$

where V' is the volume of the heat source.

The mean temperature increase of a hot disk sensor with m spirals is given by

$$\overline{\Delta T(\tau)} = \frac{1}{(m+1)\pi r_a} \frac{P_0}{2\pi^{3/2} r_a m(m+1)\lambda} \int_0^\tau \frac{\mathrm{d}\sigma}{\sigma^2} \sum_{k=1}^{m} \frac{\alpha r_a}{m} \times \sum_{k=1}^{m} l \exp\frac{-((k^2/m^2)+(l^2/m^2))}{4\sigma^2} I_0\left(\frac{kl}{2m^2\sigma^2}\right) 2\pi = \frac{P_0}{\pi^{3/2} r_a \lambda} D(\tau) \tag{4}$$

with $D(\tau)$ defined as

$$D(\tau) = \frac{1}{m^2(m+1)^2} \int_0^\tau \frac{\mathrm{d}\sigma}{\sigma^2} \sum_{k=1}^{m} k \sum_{k=1}^{m} l \exp\frac{-((k^2+l^2)/m^2)}{4\sigma^2} I_0\left(\frac{kl}{2m^2\sigma^2}\right) \tag{5}$$

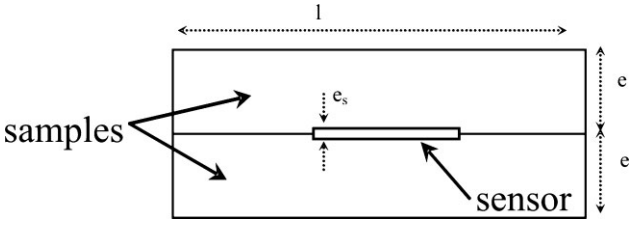

Figure 4. Hotdisk measurement principle.

$\tau = \sqrt{at}/r_a$ is called characteristic time and $\sigma^2 = a(t-t')/r_a^2$.

The temperature variation as a function of $D(\tau)$ can be represented by a straight line with slope $P_0/\pi^{3/2} r_a \lambda$, allowing a direct calculation of the thermal conductivity. However, calculation of $D(\tau)$ requires the knowledge of the thermal diffusivity that is generally unknown. An optimization process integrated to the software calculates the optimal value of the thermal diffusivity that gives a straight line for $\Delta\overline{T} = f(D(\tau))$.

The theoretical development presented before is based on the assumption of a semi-infinite sample (while in reality the samples have limited dimensions). Therefore, it is necessary to verify that, during measurements, the sample boundaries effects on the thermal distribution are negligible. For this purpose, the probing depth (Δp) defined as the distance from the sensor edge to the nearest free boundary of the sample is introduced. The influence of the sample size on the thermal conductivity measurement will be neglected if $\Delta p \geq \sqrt{4at}$.

In order to obtain identical samples (of the same dimension and the same curing rate) on both sides of the sensor, the iso-α obtained molded parts were cut in two halves.

The choice of the measurement sensor was imposed by the sample dimensions in order to be in agreement with the assumption of a semi-infinite sample. For the present work, the measurements were carried out using a hot disk sensor of 6.378 mm diameter.

The sensor was sandwiched between the two samples (Figure 4) and a slight mechanical pressure was applied to the whole system in order to improve the contact quality between the surfaces of the sensor and the sample thereby reducing the effect of the thermal resistance of contact.

Preliminary measurements allowed to determine the heating power and the duration of the measurement. These parameters were chosen in order to respect the assumption of semi-infinite medium, the conditions of measurement of temperature rise and time characteristic.

The thermal conductivity was then obtained by averaging the results of five measurements for each sample with a time interval between measurements allowing the sample to be back to thermal equilibrium.

According to HotDsik, a reliable result has to respect three criteria: the penetration depth must be lower than the sample's thickness, the characteristic time should be included between 0.3 and 1 s and the sample's temperature increase must be less than 3 K. During our measurements we noticed that, despite complying with these three criteria, the measured thermal conductivity values can vary from a measurement area to another for the same sample. In fact, the measurements were very sensitive to the surface quality of the sample and the possible presence of air bubbles on the molded part. A poor surface quality can increase considerably the thermal contact resistance.

Figure 5 presents the residual for measurements carried on two samples of the same rubber molded part and with good surface qualities. The residual represents the difference between the measured temperatures and the temperatures calculated using the estimated thermal conductivity. One of the two samples contained air bubbles (Figure 6). For the perfect sample, the residual is well centered and does not present any deviation or oscillation [Figure 5a] which is not the case for the sample containing air bubbles [Figure 5b]. The residual quality is a further criterion for the estimation reliability. Consequently, the choice of the measurement location in the molded part is of great importance for the measurements optimization.

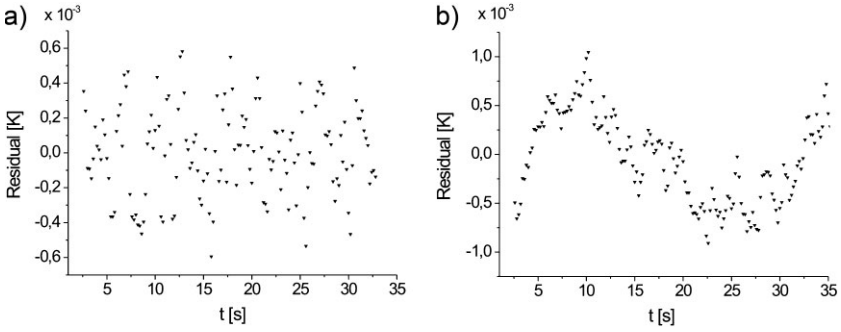

Figure 5. Residuals for a perfect sample (a) and for a sample with air bubbles (b).

This last criterion associated to the three criteria indicated by the HotDisk software allows the selection of the best test locations on the parts for which measurements are reliable.

Results and Discussion

The molding of the iso-α samples is a crucial step since the curing states are a direct result of the heating cycles determined numerically and applied by the mold regulation system on the mold cavity boundaries. The Figure 7 shows the temperature setup calculated in the case of the molding of an iso-α sample with an average vulcanization rate of 0.3.

Figure 7 shows a comparison between the programmed temperature (T_{prog}) and the temperatures recorded with two thermocouples placed on the upper (T_{up}) and the lower face (T_{low}) of the rubber part during molding process. We observe that the curing cycles really applied on the molded part surfaces are slightly different from the programmed ones due to the mold thermal inertia and the various heat losses.

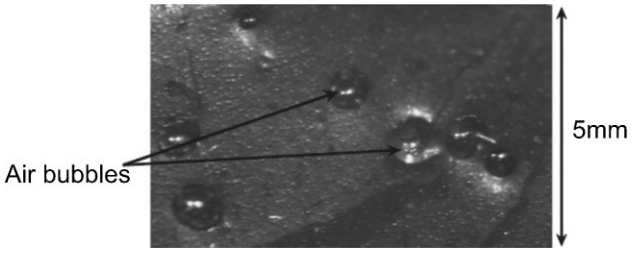

Figure 6. Molded sample containing air bubbles.

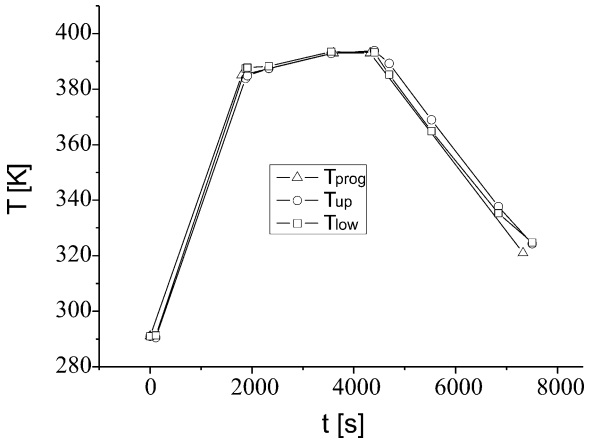

Figure 7. Comparison between programmed temperatures and real curing cycle for molded part.

The temperature differences seemingly small may affect significantly the final state of cure of the molded sample. In order to improve the vulcanization rate prediction, we use the measured temperatures (T_{up} and T_{low}) instead of the programmed ones (T_{prog}, Figure 2) as boundary conditions on the COMSOL model.

Figure 8 shows the dispersion of the vulcanization rate through the part's thickness for the four molded samples (where "meas." is the calculated vulcanization rate using the measured temperatures). We note that the state of cure is uniform for each sample and the vulcanization rate dispersion through the molded samples is minimal.

Table 2 shows the difference between curing rates of the parts (calculated using T_{up} and T_{low}) and those calculated using T_{prog}. The gap between the real curing rates and the desired ones is maximal for a vulcanization target rate

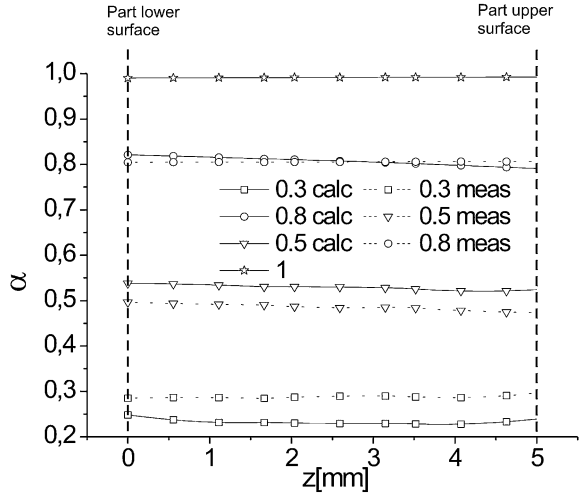

Figure 8. Dispersion of the vulcanization rate through the part thickness (z) at $r = 0$.

Table 2. Curing rates calculated with the different boundaries conditions.

α_i (target)	$\bar{\alpha}_i$ (calculated)	Standard deviation	Uncertainty [%]
0	0	0	0
0.25	0.232	0.0049	2.11
0.5	0.529	0.0053	1.01
0.8	0.807	0.0088	1.09
1	0.991	0.0006	0.06

$\alpha_i = 0.25$ and decreases for the higher levels of state of cure. This result can be explained by the high speed of the vulcanization kinetics at low reaction rates (Figure 9).

The real state of cure of each sample is estimated by measuring the residual enthalpies E_i. From the DSC measurement results presented in Figure 10, we note that the vulcanization reaction energy is very low even for a raw sample ($8.96\,J \cdot g^{-1}$) and consequently, the residual enthalpies are difficult to measure for partially cured samples. This problem can be solved, in part, by using a relatively high heating rate in the DSC measurement protocol ($20\,^{\circ}C \cdot min^{-1}$ in our case) which allows an amplification of the detected signal. Furthermore, increasing the sample mass in the crucibles will increase the measured heat amount. However, for the raw and partially cured samples ($\alpha_i = 0$, 0.25, and 0.5) an important sample weight cannot be used as the curing process goes on during the DSC measurement cycle causing the dilatation of the sample, the deformation of the pan and an important heat signal loss. For the sample with a vulcanization rate $\alpha_i = 0.8$, the curing is advanced enough to use an important mass sample. The configuration of the Perkin-Elmer 8500 DSC furnaces completely surrounding the pans provides optimal recovery of the thermal signal.

The vulcanization rate $\tilde{\alpha}_i$ of each sample is calculated by using the ratio between the residual enthalpy (E_i) and the

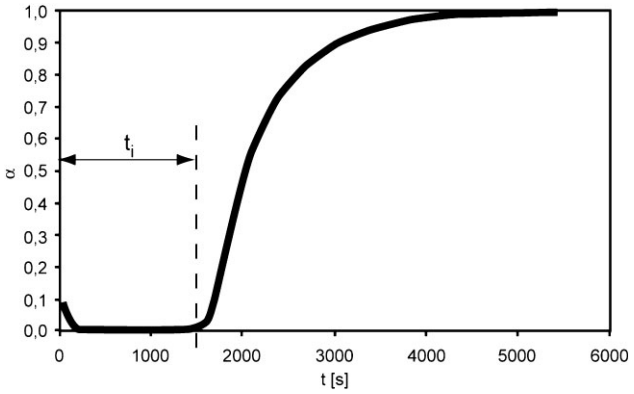

Figure 9. Rubber vulcanization kinetic.

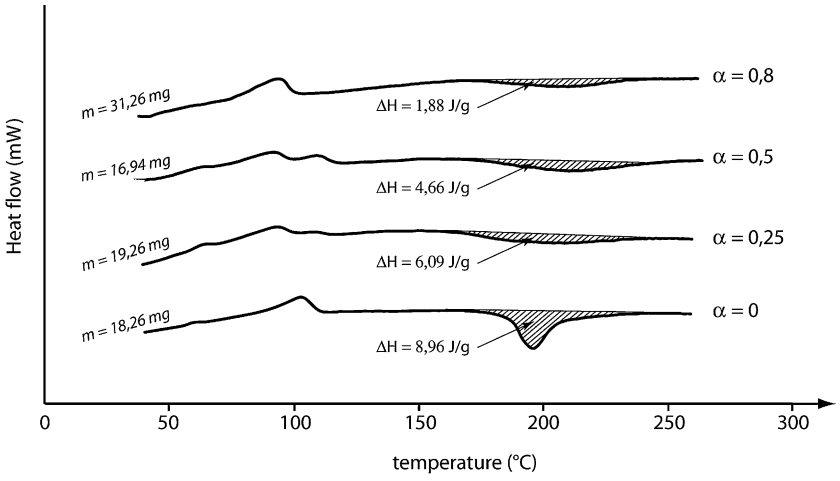

Figure 10. Measured enthalpies of iso-α samples.

total enthalpy measured for a non-vulcanized sample E_0 (Equation 1),

$$\tilde{\alpha}_i = \frac{E_0 - E_i}{E_0} \quad i \in \{0.25, 0.5, 0.8\} \tag{6}$$

Table 3 shows a comparison between target vulcanization rates (α_i), vulcanization rates calculated with the real recorded temperatures ($\bar{\alpha}_i$) and those determined by DSC measurements ($\tilde{\alpha}_i$).

We notice, in agreement with the results presented en Figure 8, that the difference between the calculated vulcanization rates $\bar{\alpha}_i$ and the measured ones $\tilde{\alpha}_i$ is maximum for a target vulcanization rate $\alpha_i = 0.25$. The high speed of the reaction makes it more difficult to control the vulcanization rate due to greater influence of the temperature variation. These conclusions comply with the results presented by Karam[30] and Dimier[31] (Figure 11) for which the uncertainties on the vulcanization rate measurement was maximal around a vulcanization rate of $\alpha = 0.25$.

The thermal conductivities of the iso-α molded parts measured by the HotDisk TPS 2500 are presented in Table 4 and the effect of the curing state on the thermal conductivity variation is presented in Figure 12.

Table 3. Calculated vulcanization rate $\bar{\alpha}_i$ and DSC-measured vulcanization rate $\tilde{\alpha}_i$.

α_i	$\bar{\alpha}_i$	$\bar{\alpha}_i/\alpha_i$ [%]	$\tilde{\alpha}_i$	$\tilde{\alpha}_i/\alpha_i$ [%]	$\tilde{\alpha}_i/\alpha_i$ [%]
0.25	0.23	8.7	0.32	21.9	28.1
0.50	0.53	5.7	0.45	11.1	17.8
0.80	0.81	1.2	0.79	1.3	2.5
1	1	0	1	0	0

The results show a significant increase of the thermal conductivity versus vulcanization rate despite the uncertainties with an average variation of the thermal conductivity is of 9.25% between the non-vulcanized compound and the totally cured one.

The result is new and we propose, in the following, to quantify the impact of this change on the prediction of the progress of the vulcanization kinetic.

Figure 13 and 14 show the effect of the thermal conductivity variation on the vulcanization kinetics progress in the case of a thick rubber part representative of an industrial one. On these figures, the vulcanization rates are calculated in three configurations. In the first configuration, the calculations are carried out with a constant thermal conductivity of a non-vulcanized rubber ($\lambda_{\alpha=0}$).

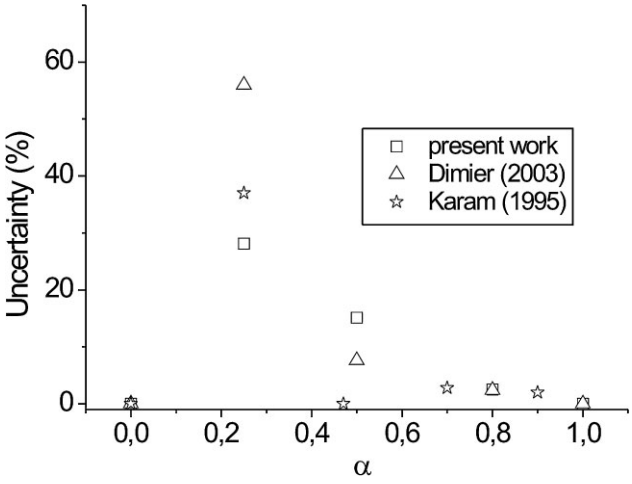

Figure 11. Error between the measured and calculated vulcanization rate.

Table 4. Measured thermal conductivities.

α_i	λ [W · m^{-1} · K^{-1}]	Standard deviation[a)] [W · m^{-1} · K^{-1}]	Uncertainty [W · m^{-1} · K^{-1}]
0	0.191	4.5×10^{-4}	0
0.25	0.199	20.6×10^{-4}	±0.0049
0.5	0.205	7.1×10^{-4}	±0.0053
0.8	0.208	3.2×10^{-4}	±0.0088
1	0.211	3.3×10^{-4}	±0.0006

[a)] Five measurements/sample.

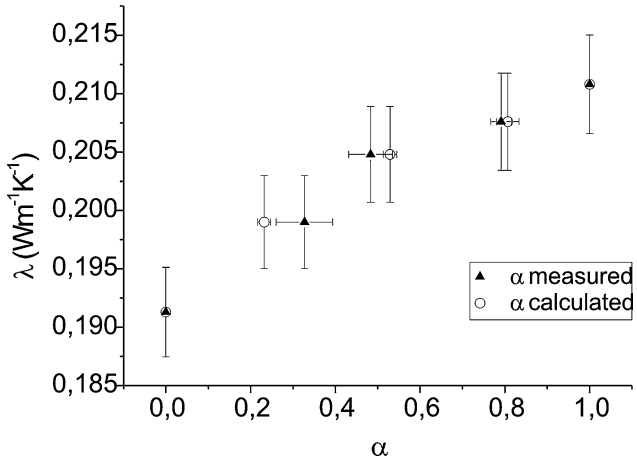

Figure 12. Effect of the vulcanization rate on the variation of the thermal conductivity.

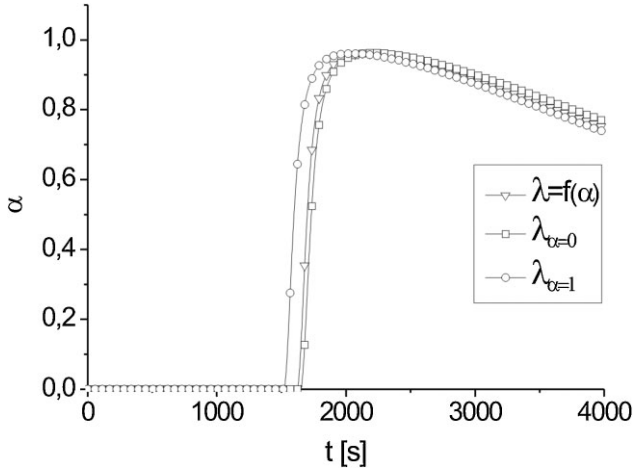

Figure 13. Effect of thermal conductivity variation as a function of α on vulcanization rate of a thick rubber part.

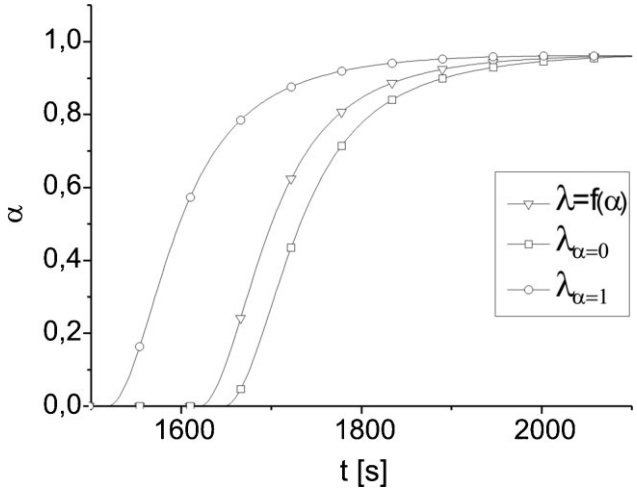

Figure 14. Effect of thermal conductivity variation as a function of α on vulcanization rate in the core of a thick rubber part.

The second configuration deals with calculations performed using a constant thermal material parameter corresponding to fully cured rubber ($\lambda_{\alpha=1}$). Finally, the third configuration, we use a thermal conductivity depending on the vulcanization rate according to Figure 12,

$$\begin{cases} t < t_i & \lambda(\alpha) = \lambda_{\alpha=0} \\ t > t_i & \lambda(\alpha) = \lambda_{\alpha=0} + 0.0195\,\alpha \end{cases} \quad (7)$$

where t_i is the induction time (Figure 6).

Figure 13 shows the effect of the α-dependence of the thermal conductivity on the vulcanization rate calculated for a thick rubber part. We note that the vulcanization rate calculated with a thermal conductivity depending on α value [$\lambda = f(\alpha)$] is closer to the vulcanization rate calculated with $\lambda_{\alpha=0}$ (of unvulcanized rubber) than that calculated with $\lambda_{\alpha=1}$ (of totally vulcanized rubber). The use of the numerical model (Figure 3) allows to build a design of experiment in order to determine the sensitivity of the vulcanization rate to the material parameters. Such tests show that the induction time value has a profound effect on the prediction of vulcanization rates. Such remark underlines the influence of the thermal conductivity on the thermal transfer calculation before the induction time.

Since the thermal conductivity depends on vulcanization only for times $t \geq t_i$, the induction times calculated for a compound with a thermal conductivity $\lambda_{\alpha=0}$ and one with a variable conductivity $\lambda = f(\alpha)$ are the same. The kinetics progress difference between the two simulations is, then, only due to the thermal conductivity variation. Thus, if the measurement of the thermal conductivity as a function of the vulcanization rate is difficult to obtain, the calculations with the thermal conductivity of a non-vulcanized rubber compound are more representative than those with thermal conductivity of a totally cured rubber.

Figure 14 shows that the effect of the λ variation is more important at the beginning of the vulcanization process, where the value of the reaction rate is the most important and the heat transfer is a non-steady one.

This point explains why, in the case of a thick part ($e = 30$ mm in our calculations), the induction time calculated with $\lambda_{\alpha=0}$ is higher than the one calculated with $\lambda(\alpha)$ [Figure 14]. In fact, during the curing of a thick part, the temperature gradient within the rubber compound modifies the thermal history at each point. The rubber located close to the part boundaries is vulcanized earlier, its thermal conductivity varies and modifies thermal transfers to the core of the part. The same calculations for a thin part are presented in Figure 15, they show that the gap between vulcanization rate simulated with $\lambda_{\alpha=0}$ and the one simulated with $\lambda(\alpha)$ in the center part are much less important.

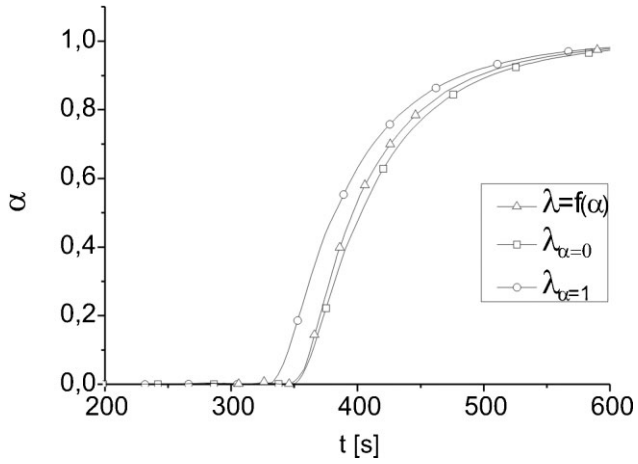

Figure 15. Effect of thermal conductivity variation as a function of α on vulcanization rate of a thin rubber part.

Conclusion

An original molding device allowing molding thick rubber parts with a homogeneous and controlled vulcanization rate has been designed and manufactured. With this device, four parts with different state of cure, 0.3, 0.5, 0.8, and 1, respectively, are molded.

The vulcanization level is validated for each part using DSC measurements of the residual curing enthalpy. These results were confirmed by numerical simulations using COMSOL software and based on the measured curing temperatures on the surfaces of parts.

The thermal conductivity of each part is measured using a HotDisk measurement system. A significant change in the thermal conductivity of rubber compound according to vulcanization is noticed. To our knowledge, such a result has not yet been reported. The impact of this dependence of thermal conductivity on the accuracy of the predictions of state of cure and temperature field during the molding process of rubber parts is shown. The results show that not taking into account the dependence of thermal conductivity depending on the cure rate can lead to significant errors on the predicted vulcanization rate.

Nomenclature

Symbol	Definition (unit)
a	Thermal diffusivity ($m^2 \cdot s^{-1}$)
C	Heat capacity ($J \cdot kg^{-1} \cdot K^{-1}$)
e	Thickness (m)
E_0	Enthalpy ($J \cdot kg^{-1}$)
E_i	Residual enthalpy ($J \cdot kg^{-1}$)
e_s	Sample thickness (m)
h	Convective heat transfer coefficient ($W \cdot m^{-2} \cdot K^{-1}$)
l	Sample length (m)
m	Ring number of sensor
Q	Heat source strength ($W \cdot m^{-3}$)
R	Electrical resistance (Ω)
R_0	Electrical resistance at T_0 (Ω)
r_a	Sensor radius (m)
T	Temperature (K)
T_0	Initial temperature (K)
$\overline{T}$	Average sample temperature (K)
t	Time (s)
t_i	Induction time (s)
z	Thickness (m)

Greek symbols

α_i	Target vulcanization rate or state of cure
$\overline{\alpha}_i$	Calculated vulcanization rate or state of cure
$\tilde{\alpha}_i$	Measured vulcanization rate or state of cure
τ	Characteristic time (s)
Δp	Probing depth (m)
α	Vulcanization rate or state of cure
λ	Thermal conductivity ($W \cdot m^{-1} \cdot K^{-1}$)
ρ	Density ($kg \cdot m^{-3}$)
υ	Temperature coefficient (K^{-1})

Subscripts

low	lower
prog	programmed
up	upper

Received: April 1, 2011; Revised: June 14, 2011; Published online: August 25, 2011; DOI: 10.1002/mame.201100127

Keywords: molding; rubber; thermal properties; vulcanization

[1] A. Cheymol, *Mise en œuvre des élastomères*, Hermès Lavoisier, Cachan **2006**.
[2] J. P. Flory, *Statistical Mechanics of Chains Molecules*, Wiley Intersciences, New York **1969**.
[3] L. R. G. Treloar, *The Physics of Rubber Elasticity*, Clarendon Press, Oxford **1958**.
[4] L. Bateman, C. G. Moore, M. Porter, B. Saville, *The Chemistry and Physics of Rubber-like Substances*, McLaren, London **1963**.
[5] J.-M. Vergnaud, I.-D. Rosca, *Rubber Curing and Properties*, CRC Press, Boca Raton **2009**.
[6] A. Ellabban, P. Mousseau, J. L. Bailleul, R. Deterre, *Inverse Probl. Sci. Eng.* **2010**, *18*, 313.
[7] D. Hands, F. Horsfall, *Rubber Chem. Technol.* **1977**, *50*, 253.
[8] P. Dashora, *Phys. Scr.* **1994**, *49*, 611.
[9] O. Sandberg, G. Bäckström, *J. Appl. Phys.* **1979**, *50*, 4720.
[10] W. Reese, *J. Appl. Phys.* **1966**, *37*, 3227.
[11] D. E. Kline, *J. Polym. Sci.* **1961**, *50*, 441.
[12] R. E. Barker, R. Y. S. Chen, R. S. Frost, *J. Polym. Sci. Part B: Polym. Phys.* **1977**, *15*, 1199.

[13] Z. I. Zaripov, G. K. Mukhamedzyanov, S. A. Bulaev, *Teplofizika Vysokikh Temperatur.* **2010**, *48*, 141.
[14] A. A. Koptelov, *Instrum. Exp. Tech.* **2003**, *46*, 842.
[15] V. P. Privalko, N. A. Rekhteta, *J. Therm. Anal. Calorim.* **1992**, *38*, 1083.
[16] P. Andersson, G. Bäckström, *J. Appl. Phys.* **1973**, *44*, 2601.
[17] Y. P. Mamunya, V. V. Davydenko, P. Pissis, E. V. Lebedev, *Eur. Polym. J.* **2002**, *38*, 1887.
[18] S. Goyanes, C. C. Lopez, G. H. Rubiolo, F. Quasso, A. J. Marzocca, *Eur. Polym. J.* **2008**, *44*, 1525.
[19] D. Hands, *Rubber Chem. Technol.* **1977**, *50*, 480.
[20] A. El Labban, P. Mousseau, R. Deterre, J. L. Bailleul, A. Sarda, *Measurement* **2009**, *42*, 916.
[21] J. S. Deng, A. I. Isayev, *Injection Molding of Rubber Compounds: Experimentation and Simulation*, American Chemical Society, Akron, USA **1991**.
[22] S. E. Gustafsson, E. Karawacki, M. N. Khan, *J. Phys. D: Appl. Phys.* **1979**, *12*, 1411.
[23] S. E. Gustafsson, E. Karawacki, M. A. Chohan, *J. Phys. D: Appl. Phys.* **1986**, *19*, 727.
[24] S. E. Gustafsson, *Rigaku J.* **1987**, *4*, 16.
[25] ISO 22007-2, Plastics – Determination of thermal conductivity and thermal diffusivity part 2: transient plane heat source (hot disc) method, 332, 2008.
[26] S. E. Gustafsson, *Rev. Sci. Instrum.* **1991**, *62*, 797.
[27] N. S. Saxena, P. Pradeep, G. Mathew, S. Thomas, M. Gustafsson, S. E. Gustafsson, *Eur. Polym. J.* **1999**, *35*, 1687.
[28] B. M. Suleiman, presented at *4th WSEAS Int. Conf. on Heat Transfer, Thermal Engineering and Environment*, Elounda, Greece, August 21–23, 2006.
[29] Y. He, *Thermochim. Acta* **2005**, *436*, 122.
[30] S. Karam, *Ph. D. Thesis*, Mines Paristech, Paris 1995.
[31] F. Dimier, *Ph. D. Thesis*, Mines Paristech, Paris 2003.